crystals

MDPI

Article

Strength of Alkane–Fluid Attraction Determines the Interfacial Orientation of Liquid Alkanes and Their Crystallization through Heterogeneous or Homogeneous Mechanisms

Yuqing Qiu and Valeria Molinero *

Department of Chemistry, The University of Utah, 315 South 1400 East, Salt Lake City, UT 84112-0850, USA
* Correspondence: Valeria.Molinero@utah.edu; Tel.: +1-801-585-9618

Academic Editor: Hiroki Nada
Received: 2 February 2017; Accepted: 9 March 2017; Published: 15 March 2017

Abstract: Alkanes are important building blocks of organics, polymers and biomolecules. The conditions that lead to ordering of alkanes at interfaces, and whether interfacial ordering of the molecules leads to heterogeneous crystal nucleation of alkanes or surface freezing, have not yet been elucidated. Here we use molecular simulations with the united-atom OPLS and PYS alkane models and the mW water model to determine what properties of the surface control the interfacial orientation of alkane molecules, and under which conditions interfacial ordering results in homogeneous or heterogeneous nucleation of alkane crystals, or surface freezing above the melting point. We find that liquid alkanes present a preference towards being perpendicular to the alkane–vapor interface and more parallel to the alkane–water interface. The orientational order in the liquid is short-ranged, decaying over ~1 nm of the surface, and can be reversed by tuning the strength of the attractions between alkane and the molecules in the other fluid. We show that the strength of the alkane–fluid interaction also controls the mechanism of crystallization and the face of the alkane crystal exposed to the fluid: fluids that interact weakly with alkanes promote heterogeneous crystallization and result in crystals in which the alkane molecules orient perpendicular to the interface, while crystallization of alkanes in the presence of fluids, such as water, that interact more strongly with alkanes is homogeneous and results in crystals with the molecules oriented parallel to the interface. We conclude that the orientation of the alkanes at the crystal interfaces mirrors that in the liquid, albeit more pronounced and long-ranged. We show that the sign of the binding free energy of the alkane crystal to the surface, ΔG_{bind}, determines whether the crystal nucleation is homogeneous ($\Delta G_{\mathrm{bind}} \geq 0$) or heterogeneous ($\Delta G_{\mathrm{bind}} < 0$). Our analysis indicates that water does not promote heterogeneous crystallization of the alkanes because water stabilizes more the liquid than the crystal phase of the alkane, resulting in $\Delta G_{\mathrm{bind}} > 0$. While $\Delta G_{\mathrm{bind}} < 0$ suffices to produce heterogeneous nucleation, the condition for surface freezing is more stringent, $\Delta G_{\mathrm{bind}} < -2\,\gamma_{\mathrm{xl}}$, where γ_{xl} is the surface tension of the liquid–crystal interface of alkanes. Surface freezing of alkanes is favored by their small value of γ_{xl}. Our findings are of relevance to understanding surface freezing in alkanes and to develop strategies for controlling the assembly of chain-like molecules at fluid interfaces.

Keywords: surface ordering; chain molecules; homogeneous nucleation; heterogeneous nucleation; surface freezing; complete wetting; assembly; crystallization

1. Introduction

Alkanes are simple organic molecules and the main building block of complex organic compounds, including surfactants, polymers and lipids. One of the unique properties of alkanes is the surface

freezing effect [1–3]. Linear alkanes with 16 to 50 carbons form a crystalline monolayer with the molecules perpendicular to the alkane–vapor interface at temperatures up to three Kelvin above their bulk equilibrium melting temperatures [2]. A recent experimental and simulation study of supercooled alkane droplets demonstrates that alkanes crystallize heterogeneously at the alkane–vapor interface [4]. A monolayer of alkanes perpendicular to the interface is formed before the interior of the droplet crystallizes [4], even for alkanes that are too short to present surface freezing.

There is no surface freezing of alkanes at the alkane–water interface [5], although alkanes interact more strongly with water than with alkane vapor. The order of alkanes at the alkane–water interface has been studied with total internal reflection second-harmonic generation spectroscopy [6–8]. The calculated effective second-order susceptibilities from simulations of configurations having the alkane chains parallel to the alkane–water interface result in better agreement with experimental measurements than the ones calculated from configurations with the alkane chains perpendicular to the interface [9]. That result is consistent with previous molecular simulations of alkane–water slabs that found the alkane to be more parallel at the interface than in the bulk of the liquid [10,11]. The first goal of this study is to identify which property controls the interfacial ordering of alkanes.

A recent simulation study of the heterogeneous crystallization of alkanes by silicon-like templating model surfaces indicates that the rate of crystallization increases as the alkane–surface interaction potential becomes more attractive [12]. As vacuum, that has no attraction to alkanes, promotes the heterogeneous crystallization of alkanes, this poses the question of whether the same rule applies to crystallization of alkanes by fluid interfaces, which cannot act as a template to order the alkane crystal. To the best of our knowledge, it has not been demonstrated whether alkanes crystallize at the water interface, with which they experience dispersion interactions. Our second goal is to determine the crystallization mechanism—homogeneous or heterogeneous—of alkanes in the presence of water and other fluids.

A commonality of surface freezing and heterogeneous crystallization of alkanes is that a layer of crystalline alkane perpendicular to the interface precedes the bulk crystallization [2,4]. The third goal of this study is to interpret the conditions that lead to homogeneous or heterogeneous nucleation of supercooled alkanes, and the existence of surface freezing above their melting point. We have recently demonstrated that the condition for heterogeneous nucleation is that the binding free energy of the crystal to the nucleating surface is negative, $\Delta G_{\text{bind}} < 0$, and that complete wetting of the surface by the crystal is attained when the binding free energy is not only negative but less than twice the liquid–crystal surface tension, $\Delta G_{\text{bind}} < -2\,\gamma_{\text{xl}}$ [13]. Here we use the framework of ref [13] to interpret the mechanism of crystallization of alkanes at fluid interfaces, and to explain why—for a particular combination of surface and alkane—heterogeneous nucleation can occur without surface freezing but surface freezing cannot occur without heterogeneous nucleation.

2. Methods

Force fields. Alkanes are modeled with two different united-atom (UA) force fields: PYS [14–16] and OPLS [17,18]. These force fields have been widely used to investigate the structure, interfacial properties and phase transitions of alkanes [4,12,19–37]. Water is modeled with the monatomic water model, mW [38], which has been extensively used to study the structure, thermodynamics, interfacial properties, and phase transitions of water [38–83]. All the force fields in this study are united-atom force fields and all interactions are short-ranged. We model the interaction of methyl and methylene groups with water through Lennard-Jones potentials, and assume that both alkane moieties, which we here call C, interact identically with water. The C–C and C–mW interactions are cut off at 1.2 nm with a long-range van der Waals tail correction to the energy and pressure [84] (implemented in LAMMPS [85] through the pair_modify tail command) as recommended for PYS alkanes in [22]. The strength and size of the mW water and OPLS nonane interaction were parameterized in ref [37]. The size of water–carbon interaction was taken as the average of SPC/E water–water distance [86] and OPLS methylene–methylene distance [18], $\sigma_{\text{wc}} = 0.35$ nm, and the strength of the water–carbon interaction,

ε_{wc} = 0.17 kcal·mol^{-1}, was parameterized to reproduce the experimental liquid water–liquid nonane surface tension γ_{lw} [37]. Here we follow the same procedure to parameterize ε_{wc} for mW water and PYS alkanes by matching the liquid–liquid surface tension γ_{lw} of nonane–water, hexadecane–water and eicosane–water to their experimental counterparts [87,88], assuming that σ_{wc} = 0.35 nm. The optimized strength of interactions between mW water and PYS alkanes ε_{wc} are 0.22, 0.20, 0.19 kcal·mol^{-1} for nonane (C9), hexadecane (C16) and eicosane (C20), respectively.

Simulations settings. We perform molecular dynamic simulations using LAMMPS [85]. The equations of motions are integrated with the velocity Verlet algorithm with timestep of 5 fs. The simulation cell is periodic in the three directions. Except when otherwise is indicated, we control the temperature and pressure using the Nose-Hoover [89,90] thermostat and barostat with time constant of 0.5 ps and 1.25 ps, respectively.

Properties. The melting temperatures of alkanes, T_m, are determined through phase coexistence in the *NpT* ensemble, following the procedure of ref [22,23]. The simulation cells contain 960 nonane molecules (C9), or 1024 hexadecane molecules (C16), or 1024 eicosane molecules (C20). We start with crystalline alkane structures from the Cambridge Structural Database [91], and we equilibrate the alkane crystals at 10 K below their corresponding T_m in the models for over 2 ns in the *NpT* ensemble. We then melt half of the simulation cell, exposing to the liquid the (100) or (001) faces of the crystals. The error bar of T_m is determined as the gap between the highest temperature at which the simulation cell crystallizes and the lowest temperature at which it melts.

The enthalpy of fusion of nonane modeled with OPLS and PYS at their corresponding melting temperature T_m, is calculated as the enthalpy difference between liquid and crystalline alkanes, $\Delta H_m = H_{liquid} - H_{crystal}$, computed from one-phase simulations of cells with 960 nonane molecules (C9), or 1024 hexadecane molecules (C16), or 1024 eicosane molecules (C20), at their corresponding T_m. The entropy of fusion ΔS_m at T_m is calculated from the enthalpy of fusion and the melting temperature, $\Delta S_m = \Delta H_m / T_m$. The enthalpies of vaporization, ΔH_{vap}, at 298 K, are calculated as the enthalpy difference between gas and liquid alkanes, $\Delta H_{vap} = H_{gas} - H_{liquid}$, where the enthalpy of the gas was computed from simulation of one gas molecule in a 7 nm × 7 nm × 14 nm simulation cell in the *NVT* ensemble with the a Langevin thermostat [92], with a damping constant of 1 ps.

The surface tension of the liquid alkane–vacuum interface, γ_{lv}, and liquid alkane–liquid water, γ_{lw}, are calculated through the mechanical route [93], as $\gamma = (L_z/2)(<p_n> - <p_t>)$, where $<p_n>$ and $<p_t>$ are the pressure tensors normal and tangential to the interface, averaged over 50 ns of *NVT* simulations, and L_z is the length of the simulation cell in the direction perpendicular to the interfaces. The simulation cells used for calculating γ_{lv} contain slabs of 114 nonane molecules, or 64 hexadecane molecules, or 120 eicosane molecules. The simulation cells used for calculating γ_{lw} contain 114 nonanes + 1024 waters, or 64 hexadecanes + 1024 waters, or 120 eicosanes + 2048 waters. The *xyz* dimensions of the simulation cells for the alkane/vacuum and alkane/water two-phase systems are identical: 3.5 nm × 3.5 nm × 7 nm for nonane, 6 nm × 6 nm × 6 nm for hexadecane and 4 nm × 4 nm × 8 nm for eicosane. The alkane molecules occupy about half of the cell, with the alkane–vacuum interface parallel to the *xy* plane. To verify that the simulation cells are sufficiently large, we also compute the surface tension of the nonane–vapor and hexadecane–vapor interfaces using 8 times larger simulation cells (with twice thicker slabs of alkane), finding identical results.

To measure the orientation of liquid alkanes at their liquid–vapor interface and liquid alkane–water interface, we run simulations in the *NVT* ensemble of OPLS nonane/mW water or PYS nonane/mW water with various ε_{wc} above the melting temperature of their corresponding alkane model. The simulation cells contain 912 nonanes (all in the liquid phase) or 912 nonanes plus 4096 waters (each in its respective liquid phase). Each periodic cell has two equivalent alkane/vapor or alkane/water interfaces. We define an end-to-end (methyl-to-methyl) vector for each nonane molecule and measure the angle θ it forms with respect to the normal to the interface. The use of the end-to-end vector to characterize the orientation of nonane assumes that the chains are extended and unbent, which is the case for nonane, although it may not be the case for long alkanes. We locate the vector

at the center of the chain. We divide the box along the surface normal into 0.1 nm wide bins, and average the θ in each bin over 20 ns simulations. For OPLS nonane we compute the orientation of the liquid at 310 K and for PYS nonane at 240 K, which correspond to 3 and 20 K above the corresponding melting points when exposing the (100) face of the crystal to the liquid (see Results section). We cannot run the simulation with PYS nonane closer to its melting point because the dynamics of the alkane become too slow to allow ergodic sampling of the molecular orientations in tens of nanoseconds. To assess the effect of water–alkane interaction on the interfacial ordering of alkanes, we perform two-phase simulations of water–alkane in which we tune the strength of ε_{wc} while keeping the original water–water and alkane–alkane interactions unchanged.

Crystallization of alkanes. We run simulations of the liquid alkane–vacuum and liquid alkane–water two-phase systems under supercooled conditions in the *NpT* ensemble to crystallize the alkanes. Crystallization of PYS hexadecane is simulated in a slab of 1024 hexadecanes in contact with vacuum or two-phase 1024 hexadecanes/8192 waters at 240 K. Crystallization of OPLS nonane is simulated in a slab of 114 nonanes in contact with vacuum or two-phase 114 nonanes/1024 waters at 270 K. The maximum waiting time for crystallization in each simulation is 100 ns. To assess the effect of water–alkane attraction on the mechanism of crystallization of alkanes, we perform simulations of crystallization, same as described above for water–alkane but in which we tune the strength of ε_{wc} while keeping the original water–water and alkane–alkane interactions. We apply the local bond order parameter q_6 [94] to distinguish crystalline from liquid hexadecane, following ref [21]. We select the largest crystalline cluster by applying the criteria that a molecule belongs to the crystal if $q_6 > 0.3$ for any six consecutive atoms in a single alkane molecule.

3. Results and Discussion

3.1. Thermodynamic Properties of the Models

3.1.1. Thermodynamics of Pure Alkanes

We first characterize the thermodynamic properties of alkanes modeled with OPLS and PYS force fields. We find that PYS reproduces the experimental melting temperature of nonane (C9), hexadecane (C16), and eicosene (C20) exposing the (100) face to the liquid (Table 1), in agreement with refs [22,23]. The (001) face of alkanes, which exposes the methyl ends of the molecules to the liquid, has lower surface energy than the (001) face, which exposes the side of the molecule to the liquid phase [22,23]. In principle, the melting temperature is a bulk property independent of the crystal face exposed, however in finite size simulations T_m can depend on the face exposed to the liquid [95]. PYS alkanes exposing the (001) face grow and dissolve at a slower rate than when exposing the (100) face, making it challenging to determine the melting points of PYS alkanes in cells exposing the (001) interface. We compute the melting temperatures of OPLS alkanes, which have not been previously reported, and find them to be much higher than their experimental counterparts. Moreover, the OPLS model fails to predict the rapid increase in melting temperature with chain length observed in experiments. T_m of OPLS nonane is almost 90 K above the experimental value (Table 2). T_m of OPLS hexadecane is 325 K, which is over 30 K higher than their experimental T_m. Because of the high overestimation of the melting temperatures of nonane by OPLS, we did not use this force field to compute melting temperatures for longer alkanes. We find that T_m computed for OPLS alkanes exposing the (001) face is at least 30 K higher than T_m determined with the (100) face exposed, due to finite size effects in the simulations. Larger simulation cells would be required for an accurate determination of the melting temperatures of alkanes models.

Table 1. Comparison of thermodynamic properties of PYS alkanes and their interfaces with mW water with the experimental ('exp.') counterparts.

Alkane	T_m (K) [a]	Exp. T_m (K)	γ_{lv} (mJ·m^{-2})	Exp. γ_{lv} (mJ·m^{-2})	γ_{lw} (mJ·m^{-2})	Exp. γ_{lw} (mJ·m^{-2})
Nonane	219 ± 2	219.5 ± 0.5 [b]	14 ± 1 [c]	22.70 [e]	54 ± 1 [c]	52.4 [e]
Hexadecane	289 ± 2	291 ± 1 [b]	18 ± 1 [d]	26.26 [f]	55 ± 1 [c]	55.2 [e]
Eicosane	309 ± 2	310 ± 1 [b]	19 ± 1 [d]	27.62 [f]	58 ± 1 [c]	56.7 [g]

[a] computed for cells exposing the (100) plane; [b] ref [96]; [c] at T = 295 K; [d] T = 313.15 K; [e] at T = 295 K, from ref [87]; [f] T = 313.15 K, from ref [97]; [g] at T = 295 K, from ref [88].

Table 2. Comparison of thermodynamic properties of pure PYS and OPLS nonane.

Nonane Model	T_m (K)	γ_{lv} (mJ·m^{-2})	ΔH_{vap} (kcal·mol^{-1})	ΔH_m (kcal·mol^{-1})	ΔS_m (cal K^{-1}·mol^{-1})
OPLS	307 ± 2 [a]	23 ± 1 [c]	12.70 [e]	4.25 [g]	13.9
PYS	219 ± 2 [a]	14 ± 1 [c]	11.19 [e]	3.50 [h]	15.9
Experiment	219.5 ± 0.5 [b]	22.7 [d]	11.16 [f]	3.59 [i]	16.4

[a] T_m determined with (100) interface; [b] ref [96]; [c] at T = 295 K; [d] at T = 295 K from ref [87]; [e] T = 298 K; [f] at T = 299 K from ref [98]; [g] T = 307 K; [h] T = 219 K; [i] at T = 219.5 K from ref [99].

Both the OPLS and PYS models underestimate the entropy of melting of the alkanes. The ability of PYS to reproduce the experimental ΔH_m and ΔS_m may be dependent on whether the alkane has an odd or even number of carbons, because although PYS underestimates ΔH_m and ΔS_m of octane by 40% [22], we find it reproduces quite well these properties for nonane (Table 2). OPLS overestimates ΔH_m of nonane by 18%. However, due to the high melting temperature of this model it underestimates ΔS_m by at least 15% compared to the experiment (Table 2). Table 2 also shows that PYS reproduces well the vaporization enthalpy ΔH_{vap} of nonane, while OPLS overestimates it.

PYS consistently underestimates the liquid–vacuum surface tension γ_{lv} of nonane, hexadecane, and eicosane by more than 30% (Table 2). OPLS overestimates so much the melting temperatures, that it is not possible to measure the liquid–vacuum surface tensions of hexadecane and eicosane at the same temperatures as in the experiments without spontaneous crystallization of the alkanes. For OPLS nonane, γ_{lv} can be measured and reproduces well the experimental value (Table 2). However, we note that OPLS overestimates the liquid–vacuum surface tension of ethane by 20% [100], indicating that the agreement is not transferable along chain lengths. We conclude that the OPLS and PYS united-atom force fields either reproduce the liquid–crystal phase equilibrium or the liquid–vacuum surface properties of alkanes, but not both.

3.1.2. Thermodynamics of Alkane–Water Systems

The interaction between the united atom methylene and methyl groups of OPLS nonane with mW water was parameterized in [37] to reproduce the experimental surface tension of the alkane/water interface, resulting in ε_{wc} = 0.17 kcal·mol^{-1} and σ_{wc} = 0.35 nm. Here we keep σ_{wc} and follow the same strategy to parameterize ε_{wc} of PYS alkanes with mW water. We find that the strength of water–methylene (or water–methyl) interactions ε_{wc} needed to reproduce the experimental alkane–water surface tension decreases slightly (within 0.03 kcal·mol^{-1}) with the length of the PYS alkane chains (Table 1). To assess the sensitivity of the liquid-alkane-water surface tension γ_{lw} to ε_{wc}, we apply the ε_{wc} of nonane–water to the other alkanes, and find that γ_{lw} deviates from the experimental values by less than 3 mJ·m^{-2}. We do not assess here whether ε_{wc} is transferable over the chain length for OPLS alkanes, as we only model nonane with that force field. Use of different strength of water–methyl and water–methylene interactions may allow the use of a single set of parameters for all the PYS alkane–water interactions.

Although OPLS and PYS alkanes have different force field parameters and thermodynamic properties, in what follows we show that they display the same trends in the orientational order of alkanes and in the mechanism of crystallization in the presence of water or vacuum, indicating that the results of this study are robust and independent on the details of the force fields.

3.2. Interfacial Orientation of Liquid Alkanes is Controlled by the Strength of Attraction to the Other Phase

Before investigating the crystallization mechanisms of alkanes, we characterize the orientational ordering of liquid alkanes in contact with vacuum and water. We address the effect of alkane–water attraction ε_{wc} on the interfacial orientation and surface tension of the latter interface. To identify the position of the interfaces, we compute the density profile of the center of mass of the alkanes for slabs of nonane in contact with vacuum or water (Figure 1a,b) and find the Gibbs dividing surface, defined as the plane where the density reaches half the bulk value. Figure 1 shows that the density of liquid alkane peaks at about 0.5 nm from that interface. The existence of interfacial density peaks has been previously reported for other alkanes [101,102]. The density peaks are sharper at the nonane–water interface than at the nonane–vacuum interface.

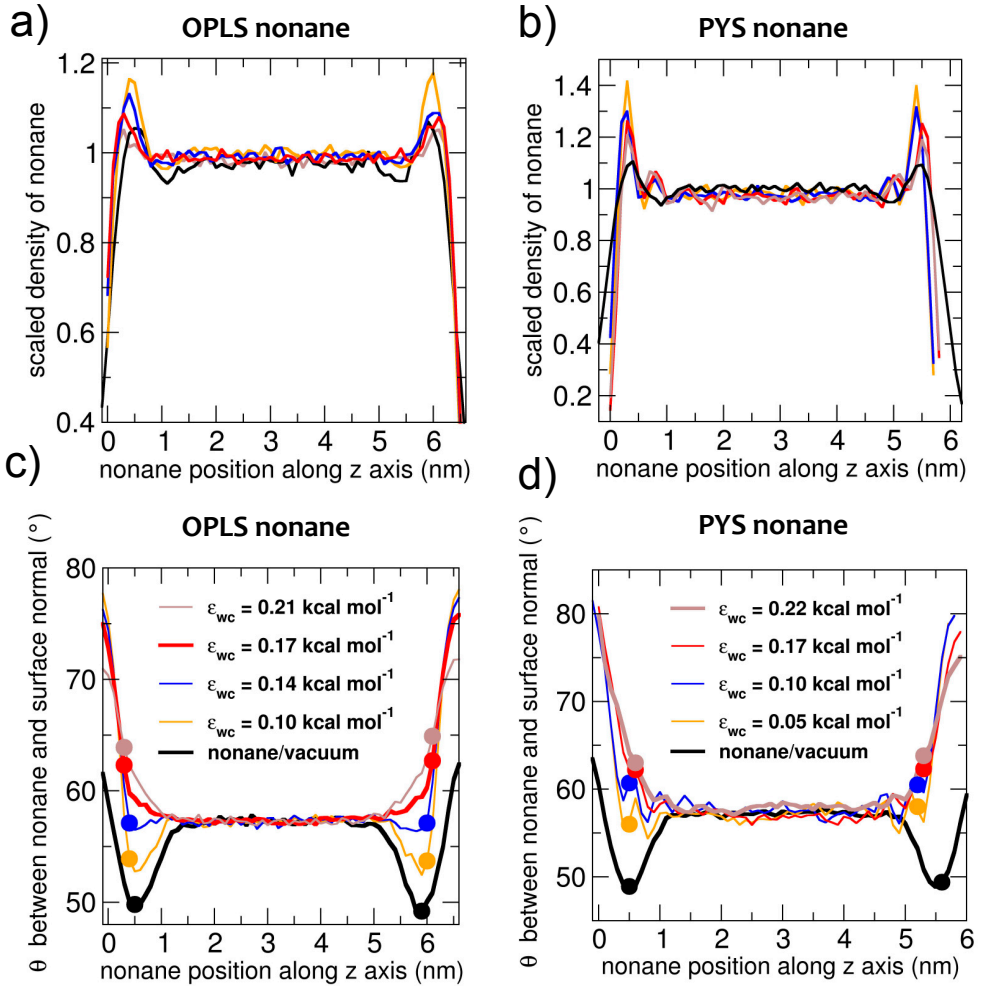

Figure 1. Profiles of the density (**a**,**b** panels) and average orientation (**c**,**d** panels) of liquid nonane in contact with vacuum and water, for which the strength ε_{wc} of the water–carbon interaction is tuned. The ordering of the liquid by the interface is short-ranged, about the length of a nonane molecule, and turns from leaning parallel to the surface to leaning more perpendicularly to the surface on decreasing the strength of the coupling between alkane and the other fluid phase (water or vacuum). The parameters that reproduce the experimental water–nonane surface tension are shown with thick lines: brown for PYS (ε_{wc} = 0.22 kcal·mol^{-1}) and red for OPLS (ε_{wc} = 0.17 kcal·mol^{-1}). The densities are presented scaled with respect to the bulk values; the orientations are computed with respect to the surface normal, as shown in Figure 2. Densities and orientations are computed at 310 K for OPLS nonane and at 240 K for PYS nonane. Solid circles signal the average orientation θ measured 0.5 nm from the Gibbs dividing surface.

To characterize the orientation of the molecules, we measure the angle θ between the methyl-to-methyl vector that each molecule forms with the normal to the interface (Figure 2): $\theta = 90^\circ$ means that the molecule is parallel to the interface and $\theta = 0^\circ$ that it is perpendicular to the interface. The orientational order of nonane at the interface is short ranged (Figure 1c,d), decaying to the bulk value at distances beyond 1.0 nm (the length of a nonane molecule) from the Gibbs dividing surface. Liquid nonane has a preference towards being perpendicular to the alkane–vacuum interface, irrespective of the force field and in agreement with what was previously reported for the orientation of a slab of OPLS decane in contact with vacuum [103,104]. At the water interface, the alkanes are more parallel compared to their average orientation in the bulk. We find that the extent of orientational order is slightly more pronounced at the vacuum than the water interface. Our results are consistent with previous simulations of GROMOS decane in contact with SPC or SPC/E water [10] and a recent interpretation of sum frequency scattering experiments of the decane–water interface [9]. We conclude that, irrespective of the force fields used for the calculations, liquid alkanes have opposite orientational preferences at the alkane–water and the alkane–vacuum interface.

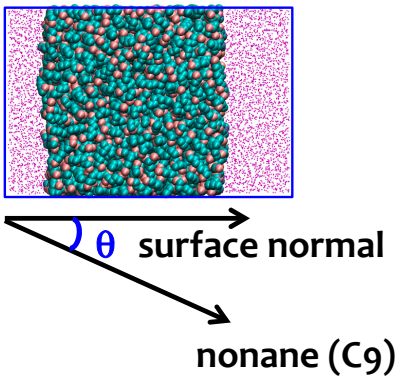

Figure 2. The orientation of the alkane molecules is characterized by the angle θ between the alkane molecules and surface normal. The upper panel shows a typical snapshot of the water–nonane simulation cell. Methyl groups are shown with pink beads and methylene groups with cyan beads. Water is represented by magenta points. Blue squares denote the periodic boundaries of the simulation box. The lower panel illustrates the relation between the angle θ and the orientation of nonane.

To understand how the strength of attraction between alkane and the other phase (which we below call solvent) impacts the interfacial orientation of liquid alkanes, we perform simulations of alkane in contact with water varying the strength of the water–carbon attraction, ε_{wc}, to span the range of the interactions from water to vacuum (Figure 1c,d). We find that the orientational preference of the alkanes at the interface evolves from parallel to perpendicular with decreasing strength of water–carbon coupling ε_{wc}. Decreasing ε_{wc} also results in a linear increase in the liquid alkane–water surface tension γ_{lw} (Figure 3). We note that in the limit of null interaction between water and the alkane, the interfacial tension of the water–alkane interface should be the sum of the water–vacuum and alkane–vacuum interfaces. In next section, we investigate whether the tuning of the interfacial ordering of the alkanes results in a change in mechanism from heterogeneous to homogeneous nucleation and distinct preference of interfacial orientation of alkanes in the crystal phase.

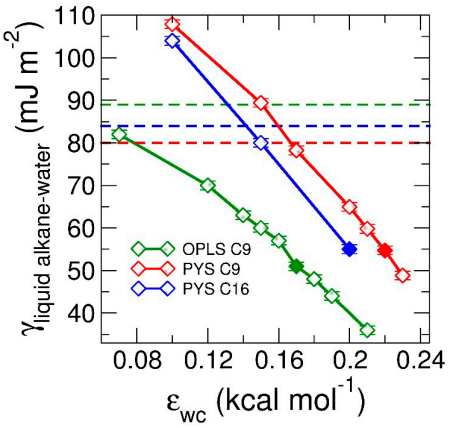

Figure 3. Surface tension of liquid alkane–water interface, γ_{lw}, as a function of the coupling between water and alkanes, ε_{wc}. Green, red, blue curves correspond to surface tensions of OPLS nonane (C9), PYS nonane (C9) and PYS hexadecane (C16), respectively. The surface tensions are computed at the same temperatures as in the experimental references: 295 K for nonane [87] and 313.15 K for hexadecane [97]. Solid squares represent the ε_{wc} at which experimental surface tension are reproduced. Note that in the limit where the water–alkane interactions become purely repulsive, the surface tension of the water–alkane interface can be larger than the sum of the surface tensions of non–interacting water–vacuum and alkane–vacuum interfaces. The latter is given by the sum of the surface tension of the water–vacuum interface (66 mJ·m^{-2} at 295 K [105]) and the liquid alkane–vacuum interfaces (Tables 1 and 2), $\gamma_{wv} + \gamma_{lv}$, and are shown with dashed lines.

3.3. Strength of the Alkane–Solvent Attraction Determines Whether Alkanes Crystallize through Heterogeneous or Homogeneous Nucleation

We study the crystallization mechanisms of nonane and hexadecane at the alkane–water and alkane–vacuum interfaces under highly supercooled conditions, at least 45 K below the corresponding T_m. Alkanes crystallize heterogeneously at the alkane–vacuum interface (Figure 4a), irrespective of the force field and in agreement with previous studies using the PYS model [4]. In the presence of water, the alkanes crystallize homogeneously, forming the critical crystal nucleus in the interior of the liquid phase (Figure 4b).

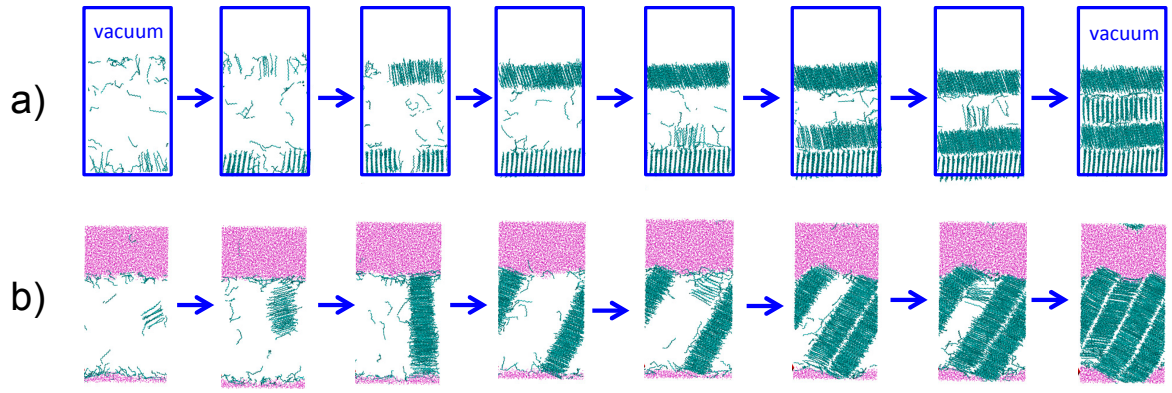

Figure 4. Snapshots of PYS hexadecane crystallizing (**a**) heterogeneously at the hexadecane–vacuum interface at 240 K and (**b**) homogeneously in the presence of water (ε_{wc} = 0.20 kcal·mol^{-1}) at 245 K. The induction time that precedes crystallization is not shown. Cyan lines indicate crystalline C16; the liquid alkane phase is hidden. Pink points represent water. Blue rectangles in (**a**) denote the boundaries of the periodic alkane/vacuum simulation box.

The nucleus of the alkane crystal has the same shape for heterogeneous and homogeneous nucleation: a cylindrical one-molecule thick bundle of partially aligned alkane chains [21,23] (Figure 4). In the presence of a vacuum interface, the crystal nucleus forms at the surface, with the molecules aligned perpendicular to the vacuum interface (Figure 4a). The crystal grows first in the direction parallel to the interface, before it nucleates and grows subsequent layers. The same mechanism has been reported for the crystallization of large PYS nonane droplets [4]. The simulations suggest that the alkane–vacuum interface stabilizes the chain-end rather than the side of the alkane molecules. The perpendicular orientation of the alkanes at the crystal–vacuum interface is consistent with the orientation in the liquid and in the one-layer-thick surface freezing in medium length alkanes.

The one-molecule thick bundle-like nucleus for the homogeneous crystallization in the presence of water grows by first adding alkanes on the side of the nucleus—which results in a one-molecule thick crystal layer—and only then growing a second crystal layer (Figure 4b). Same as in the growth in the presence of vapor, there is a separation of time scales for growth of the one-molecule thick crystal layer and the secondary nucleation and growth of subsequent layers. Irrespective of the initial orientation of the crystal nucleus, when the alkane crystal reaches the water interface, it reorients to expose the long side of the alkane molecules to water. We equilibrate this crystalline structure at the melting temperature, and find that alkanes align to maximize the hexadecane–water interface, producing a 'seesaw' shaped interface that exposes the (100) surface of the crystal to liquid water. We conclude that, same as for the vacuum interface, the orientational order of the molecules at the crystal–water interface mirrors the one in the liquid, albeit very pronounced and long ranged.

The orientations of crystalline alkanes at the alkane–water interface can be rationalized as follows. The strength of the interaction between water and CH_3 or CH_2 are the same, but the atom density on the side of the crystallized alkanes (i.e., the (100) surface) is higher than that on the end of the crystallized molecules (i.e., the (001) surface), which makes water stabilize the (denser) side face of crystalline alkanes more than their (less dense) CH_3 end. The 'seesaw' shape of the (100) interface occurs because the hexadecane molecules in the crystal are not parallel to the interface between alkane layers, which we confirm in the simulations of growth of PYS hexadecane. We note that PYS overestimates the tilt of octane in the crystal with respect to the experimental value, 120.0° in the model vs. 105.8° in the experimental crystal structure [22], and it may overestimate the tilt also for hexadecane.

An earlier simulation study of ultrathin films with less than three layers of alkanes on solid substrates showed that very attractive surfaces orient the first layer of alkanes parallel to the surface while weakly attractive surfaces orient them perpendicular [106]. We find the same trend for the surface orientation of bulk alkanes at fluid interfaces as we tune the strength of the solvent–alkane attraction ε_{wc} (Figure 3) between PYS hexadecane or OPLS nonane and water. Figure 5 shows representative snapshots of the simulation trajectories displaying crystalline alkanes for each ε_{wc} in the alkane/water systems. At low ε_{wc} the alkane molecules orient mostly perpendicular to the surface (Figure 1) and the crystallization is heterogeneous at the interface. We define as the 'neutral' ε_{wc} the one for which θ measured half a molecule length (0.5 nm) from the Gibbs dividing surface (solid circles in Figure 1c,d) is the same as in bulk. The neutral ε_{wc} depends on the force field and the length of the chain: 0.14 kcal·mol^{-1} for OPLS nonane, 0.05 kcal·mol^{-1} for PYS nonane and 0.15 kcal·mol^{-1} for PYS hexadecane. We find a transition from heterogeneous to homogeneous nucleation as ε_{wc} increases above the neutral orientation value. At the neutral ε_{wc} alkanes can either nucleate homogeneously or heterogeneously, suggesting that the crystalline nuclei have similar stabilities in the bulk and at the interface. We conclude that the attraction between alkanes and the fluid phase reverses the orientation of the crystalline alkanes with respect to the surface and controls the mechanism of crystallization.

A recent simulation study of crystallization of pentacontane (C50) finds that it crystallizes heterogeneously at solid silicon-like templating surfaces, resulting in crystals with the chains oriented parallel to the interface, and that the nucleation is faster for more strongly interacting surfaces [12,19,20]. Based on these results, it may be expected that increasing ε_{wc} between alkane and the water fluid may increase the ordering of the molecules parallel to the interface, and could result in a new

region of heterogeneous nucleation at high ε_{wc}. However, we find that increasing ε_{wc} between PYS hexadecane and water to 0.22 kcal·mol^{-1} (10% over the value for mW water–PYS C16) does not result in heterogeneous nucleation but in mixing of the two components. This suggests that different from solid crystal-templating surfaces, liquids that interact with alkanes more strongly than water would rather dissolve the alkanes than result in heterogeneous crystallization.

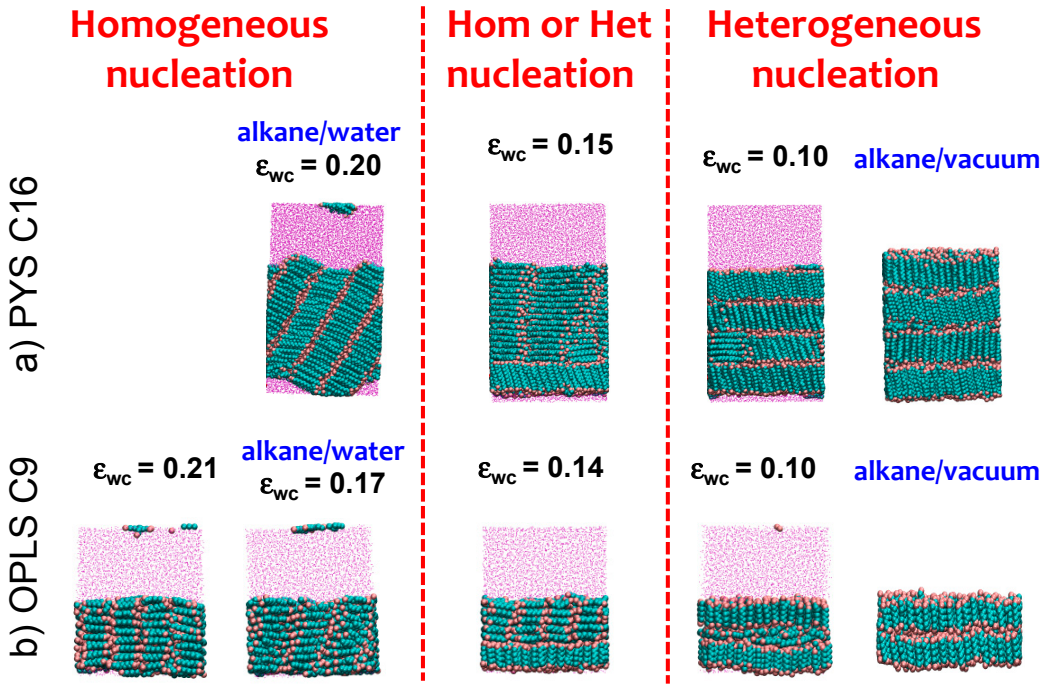

Figure 5. Interfacial orientation of (**a**) PYS hexadecane or (**b**) OPLS nonane crystallized in the presence of solvent (water or vacuum) is reversed from parallel to perpendicular by decreasing the strength of water–carbon interaction ε_{wc}. The trend does not depend on the alkane length or force field. Snapshots shown correspond to the end of the alkane crystallization in the presence of solvent with coupling ε_{wc} indicated. We highlight with blue labels the cells corresponding to the alkane/water parameters that reproduce the experimental surface tension and the alkane/vacuum systems. The change in interfacial orientation from parallel to perpendicular in the crystal coincides with the change from homogeneous to heterogeneous nucleation, and occurs for the neutral ε_{wc}, for which the orientation of the alkanes at the surface of the liquid is the same as in the bulk.

3.4. The Sign and Magnitude of the Binding Free Energy of the Alkane Crystal to the Surface Determine Whether the Crystal Nucleation is Homogeneous, Heterogeneous, or There Is Surface Freezing

In what follows we use classical nucleation theory [107] (CNT) to identify the conditions that lead to homogeneous crystal nucleation, heterogeneous crystal nucleation, and surface freezing above the equilibrium melting point. We then use that framework to rationalize why alkane crystals nucleate heterogeneously in contact with vacuum or weakly interacting fluids and homogeneously with more strongly interacting liquids, such as water.

The rate of crystal nucleation in CNT is $J = A \exp(-\Delta G^*/k_B T)$, in which the prefactor A depends mostly on the diffusion coefficient of the molecules in the liquid, ΔG^* is the free energy barrier of nucleation, k_B is the Boltzmann constant and T the temperature. The heterogeneous nucleation barrier in CNT is given by $\Delta G^*_{het} = N^* \Delta\mu + A_{xl}{}^* \gamma_{xl} + A_{xs}{}^* \Delta\gamma$, where N^* is the number of molecules in the critical nucleus, $\Delta\mu$ is the difference in chemical potential between liquid and crystal, and $A_{xl}{}^*$ and $A_{xs}{}^*$ are the areas of the liquid–crystal and surface–crystal interfaces of the critical nucleus, γ_{xl} is the surface tension of the liquid–crystal interface, and $\Delta\gamma = \gamma_{xs} - \gamma_{ls}$ is the difference between the surface tension of the crystal–surface and liquid–surface interfaces. The geometry of the nucleus is determined by

Young's equation, $\gamma_{xl}\cos\alpha + \Delta\gamma = 0$, where α is the contact angle of crystal nucleus on the surface [108]. Heterogeneous nucleation can only be induced when $\cos\alpha > -1$, which implies that the binding free energy of the crystal nucleus to the surface is negative, $\Delta G_{bind} = \gamma_{xs} - (\gamma_{ls} + \gamma_{xl}) < 0$ (Figure 6) [13]. Surface freezing can be considered a case of complete wetting of the surface by the crystal, which requires that $\Delta G_{bind} < -2\ \gamma_{xl}$ (Figure 6) if the line tension of the crystal–liquid–surface interface is neglected [13,109]. Heterogeneous nucleation at a surface can occur without surface freezing when $-2\ \gamma_{xl} < \Delta G_{bind} < 0$. If surface freezing occurs, then the bulk crystal will nucleate heterogeneously from the frozen interface at T_m.

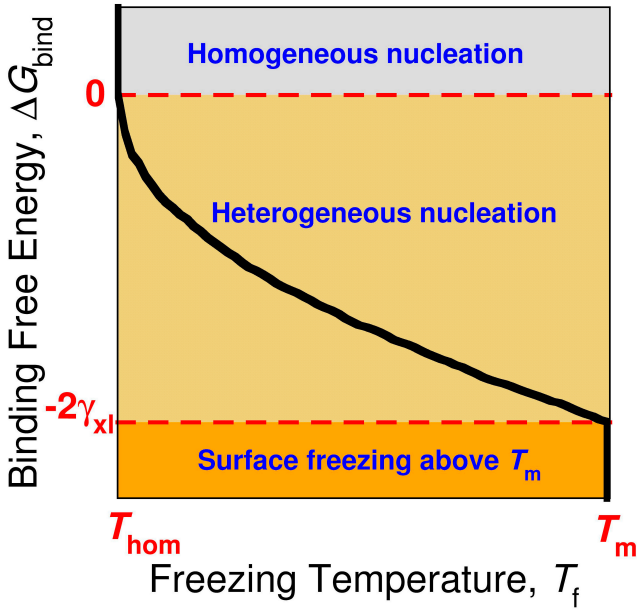

Figure 6. Sketch of the relation between the bulk freezing temperature T_f of the alkane crystal (black line) and the binding free energy ΔG_{bind} of the crystalline alkane to the nucleating surface. The curve corresponds to a constant nucleation rate, which determines the homogeneous nucleation temperature T_{hom} [13]. The sign and magnitude of ΔG_{bind} determines whether the surface can induce heterogeneous nucleation or promote surface freezing. If $\Delta G_{bind} > 0$, the crystal nucleates homogeneously at T_{hom}. For surfaces that produce $0 > \Delta G_{bind} > -2\ \gamma_{xl}$, the nucleation of the alkane crystal is heterogeneous but there is no surface freezing above the equilibrium melting temperature T_m. If $\Delta G_{bind} < -2\ \gamma_{xl}$, the surface induces surface freezing of the alkane above T_m, and the crystal nucleates heterogeneously from the frozen surface just below T_m.

Heterogeneous crystallization of the alkanes at the vapor interface implies that the crystallite is more stable at the vapor interface than in the bulk of the liquid. This happens when $\Delta G_{bind} = \gamma_{xv} - (\gamma_{lv} + \gamma_{xl}) < 0$, where γ_{lv}, γ_{xv}, and γ_{xl} are the are the surface tension of liquid–vapor, crystal–vapor and liquid–crystal interfaces for the alkanes. The liquid–crystal surface tension γ_{xl} of alkanes is in the order of a few mJ·m^{-2} in experiments and simulations [22,23]. The γ_{lv} of alkanes are 20 to 30 mJ·m^{-2}, as reported in Tables 1 and 2. The surface energy between crystal alkanes and vapor γ_{xv} has not been, to our knowledge, experimentally determined. γ_{xv} has been recently computed for PYS octane (C8) and Trappe nonadecane (C19) at their corresponding melting temperatures [30], and found to be ~40% lower for the longer alkane, 35 and 24 mJ·m^{-2} [30]. We note that for heterogeneous crystallization to occur at the vapor interface, the condition $\Delta G_{bind} < 0$ has to be satisfied at the non-equilibrium crystallization temperature, although it may not be satisfied at the melting point.

Surface freezing of alkanes at the vapor interface requires $\Delta G_{bind} = \gamma_{xv} - (\gamma_{lv} + \gamma_{xl}) < -2\ \gamma_{xl}$ [13,110,111], a requirement stronger than for hetergeneous nucleation. Since the surface tension of liquid–crystalline alkane γ_{xl} is small, a few mJ·m^{-2} [22,23], there is a narrow range of ΔG_{bind} for

which heterogeneous crystallization of alkanes at the vapor interface occurs without surface freezing. C8 satisfy this condition, and does not present surface freezing although it heterogeneously crystallizes at the vacuum interface [30]. C16 to C50 display surface freezing [1–3]. Our analysis indicates that the small free energy cost of the liquid–crystal interface γ_{xl} in alkanes is key for the realization of surface freezing at surfaces as different as vacuum [1–3] and SiO_2 [112,113].

For the crystallization of the alkanes at the water interface, the binding free energy is $\Delta G_{bind} = \gamma_{xw} - (\gamma_{lw} + \gamma_{xl})$, where γ_{xw}, and γ_{lw} are the surface tension of water in contact with crystalline and liquid alkane, respectively. While γ_{lw} is readily available from experiments or simulations (see Section 3.1), we are unable to find experimental data for the surface tension of the water–crystalline alkane interface, γ_{xw}. To interpret why the alkane–water interface cannot induce heterogeneous crystallization of alkanes, we draw a schematic diagram of the evolution of γ_{lw} and γ_{xw} with increasing ε_{wc} (Figure 7) based on the crystallization mechanism vs. ε_{wc} reported in Figure 5. We interpret that increasing ε_{wc} stabilizes the water–liquid alkane interface more than the water–crystal alkane interface, although both interfaces would be stabilized (i.e., γ_{lw} and γ_{xw} decrease) on increasing alkane–solvent attraction. This differential stabilization of γ_{lw} vs. γ_{xw} with ε_{wc} should result in a crossover between γ_{lw} and $\gamma_{xw} - \gamma_{lx}$ that, as we discussed above, signals the transition from heterogeneous to homogeneous nucleation when the interfacial liquid alkane has the same orientation as in the bulk. Our analysis indicates that liquid water does not induce heterogeneous crystal nucleation because it preferentially stabilizes the liquid phase of the alkane.

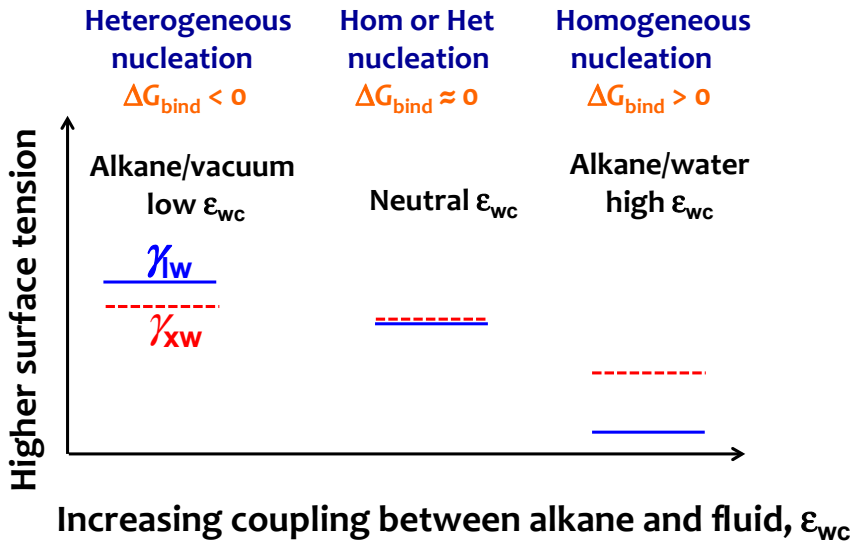

Figure 7. Scheme to interpret the change from heterogeneous to homogeneous nucleation mechanism on increasing the strength of alkane–solvent attraction ε_{wc}. The simulation trends of Figure 5 indicate that on increasing ε_{wc} the liquid alkane–water interfacial tension γ_{lw} (blue line) decreases more than the crystalline alkane–water surface tension γ_{xw} (red line), resulting in an increase of the binding free energy ΔG_{bind}. The neutral ε_{wc} signals the transition from heterogeneous to homogeneous at $\Delta G_{bind} = 0$, which coincides with the lack of preference for parallel or perpendicular orientation for the interfacial liquid alkane.

4. Conclusions

We use molecular dynamic simulations to investigate the relation between the interfacial orientation of alkanes in the liquid phase and their mechanism of crystallization. In agreement with previous simulation results [10,103,104] and the interpretation of experiments [9], we find that alkane molecules in the liquid orient in opposite directions at the vacuum and water interfaces: they preferentially align perpendicular to the vacuum interface and parallel to the water interface. However, we note that the orientation is not very pronounced: eight degrees below the bulk average for vacuum

and six degrees above the bulk average for water for PYS alkanes, and even less for the OPLS model. We demonstrate that the interfacial orientation of the alkanes in the liquid can be tuned through the strength of the fluid solvent (water) and alkane attraction. Increasing the solvent–alkane attraction results in an orientation of the alkanes more parallel to the interface.

Although both water and vacuum orient liquid alkanes at the interface, only the vacuum interface promotes heterogeneous nucleation of alkane crystals. Heterogeneous crystallization of alkanes at the vacuum interface results in crystals with molecules oriented perpendicular to the surface, same as in the critical crystal nucleus from which they grow. Crystallization of alkanes in the presence of water occurs through homogeneous nucleation in the bulk of the alkane liquid phase (Figure 4a). Although the homogeneous critical nucleus forms with an arbitrary orientation in the bulk liquid with respect to the alkane–solvent interface, as the crystal grows and reaches the water interface, the nucleus rotates and the alkane molecules in the crystal end up aligned parallel to the surface (Figure 4b), maximizing the attractive interactions between alkane and water. We conclude that the preferential orientation of alkane molecules in the crystal with respect to the fluid surface mirrors the one in liquid alkanes, although the order in the crystal is long-ranged, in the liquid it involves only the first monolayer at the interface.

Tuning the interactions of the liquid alkane–solvent interface from non-interacting vacuum-like to water values results in a change from heterogeneous to homogeneous nucleation as the orientation of the molecules in the interfacial liquid turn from leaning perpendicular to leaning parallel to the surface. Our analysis indicates that the change in mechanism results from a preferential stabilization of the liquid alkane–solvent interface compared to the crystalline alkane–solvent interface on increasing the alkane–solvent attraction.

We use Classical Nucleation Theory to explain the transition from heterogeneous to homogeneous nucleation on increasing the strength of the alkane–solvent interactions and the distinct conditions that lead to heterogeneous nucleation from the supercooled liquid and surface freezing above the equilibrium melting temperature. Heterogeneous nucleation occurs when the binding free energy of the crystal (immersed in its melt) to the nucleating surface is negative ($\Delta G_{\text{bind}} < 0$), while surface freezing requires a more stringent condition: that the binding free energy is less than minus twice the liquid–crystal surface tension of the alkane, ($\Delta G_{\text{bind}} < -2\,\gamma_{\text{xl}}$) [13,109]. This implies that there is a range of binding free energies for which heterogeneous nucleation can occur without surface freezing. This must be the case for alkanes with fewer than 16 carbons at the vacuum interface. Interestingly, silica-coated Si (100) surfaces produce surface freezing in which the alkane molecules are oriented parallel to the surface [113], opposite to the order they present at the vacuum interface [1–3]. These results stress that surface freezing can be attained by solid surfaces that interact very weakly and strongly with the alkanes. Likewise, experiments and simulations indicate that crystalline surfaces that interact strongly with alkanes can induce heterogeneous nucleation with the chains ordered parallel to the surface [12,112,113]. This region of $\Delta G_{\text{bind}} < 0$ for highly interacting surfaces cannot be accessed with a fluid interface, as we observe that increase in interaction strength results in mixing instead of heterogeneous nucleation. This distinction should be important in developing strategies to control the assembly of alkane-containing organic and biological molecules at fluid and solid interfaces.

Acknowledgments: This work was supported by the National Science Foundation through award CHE-1305427 'Center for Aerosol Impacts on Climate and the Environment'. We thank the Center for High Performance Computing at The University of Utah for technical support and a grant of computer time.

Author Contributions: Yuqing Qiu and Valeria Molinero conceived the work and wrote the paper. Yuqing Qiu parameterized the models, performed the simulations and analyzed the data.

Conflicts of Interest: The authors declare no conflict of interest.

References

1. Wu, X.; Sirota, E.; Sinha, S.; Ocko, B.; Deutsch, M. Surface crystallization of liquid normal-alkanes. *Phys. Rev. Lett.* **1993**, *70*, 958–961. [CrossRef] [PubMed]

2. Ocko, B.M.; Wu, X.Z.; Sirota, E.B.; Sinha, S.K.; Gang, O.; Deutsch, M. Surface freezing in chain molecules: Normal alkanes. *Phys. Rev. E* **1997**, *55*, 3164–3182. [CrossRef]
3. Tkachenko, A.V.; Rabin, Y. Fluctuation-Stabilized Surface Freezing of Chain Molecules. *Phys. Rev. Lett.* **1996**, *76*, 2527–2530. [CrossRef] [PubMed]
4. Modak, V.P.; Pathak, H.; Thayer, M.; Singer, S.J.; Wyslouzil, B.E. Experimental evidence for surface freezing in supercooled n-alkane nanodroplets. *Phys. Chem. Chem. Phys.* **2013**, *15*, 6783–6795. [CrossRef] [PubMed]
5. Tikhonov, A.M.; Mitrinovic, D.M.; Li, M.; Huang, Z.; Schlossman, M.L. An X-ray reflectivity study of the water-docosane interface. *J. Phys. Chem. B* **2000**, *104*, 6336–6339. [CrossRef]
6. Conboy, J.; Daschbach, J.; Richmond, G. Studies of Alkane/Water Interfaces by Total Internal Reflection Second Harmonic Generation. *J. Phys. Chem.* **1994**, *98*, 9688–9692. [CrossRef]
7. Conboy, J.C.; Daschbach, J.L.; Richmond, G.L. Total internal reflection second-harmonic generation: Probing the alkane water interface. *Appl. Phys. A* **1994**, *59*, 623–629. [CrossRef]
8. Mitrinović, D.M.; Tikhonov, A.M.; Li, M.; Huang, Z.; Schlossman, M.L. Noncapillary-Wave Structure at the Water-Alkane Interface. *Phys. Rev. Lett.* **2000**, *85*, 582–585. [CrossRef] [PubMed]
9. Vácha, R.; Roke, S. Sodium Dodecyl Sulfate at Water–Hydrophobic Interfaces: A Simulation Study. *J. Phys. Chem. B* **2012**, *116*, 11936–11942. [CrossRef] [PubMed]
10. Van Buuren, A.R.; Marrink, S.J.; Berendsen, H.J.C. A molecular dynamics study of the decane/water interface. *J. Phys. Chem.* **1993**, *97*, 9206–9212. [CrossRef]
11. Xiao, H.; Zhen, Z.; Sun, H.; Cao, X.; Li, Z.; Song, X.; Cui, X.; Liu, X. Molecular dynamics study of the water/n-alkane interface. *Sci. China Chem.* **2010**, *53*, 945–949. [CrossRef]
12. Bourque, A.J.; Locker, C.R.; Rutledge, G.C. Heterogeneous Nucleation of an n-Alkane on Tetrahedrally Coordinated Crystals. *J. Phys. Chem. B* **2017**, *121*, 904–911. [CrossRef] [PubMed]
13. Qiu, Y.; Odendahl, N.; Hudait, A.; Mason, R.H.; Bertram, A.K.; Paesani, F.; de Mott, P.J.; Molinero, V. Ice nucleation efficiency of hydroxylated organic surfaces is controlled by their structural fluctuations and mismatch to ice. *J. Am. Chem. Soc.* **2017**, *139*, 3052–3064. [CrossRef] [PubMed]
14. Waheed, N.; Ko, M.J.; Rutledge, G.C. Molecular simulation of crystal growth in long alkanes. *Polymer* **2005**, *46*, 8689–8702. [CrossRef]
15. Waheed, N.; Lavine, M.S.; Rutledge, G.C. Molecular simulation of crystal growth in n-eicosane. *J. Chem. Phys.* **2002**, *116*, 2301–2309. [CrossRef]
16. Paul, W.; Yoon, D.Y.; Smith, G.D. An optimized united atom model for simulations of polymethylene melts. *J. Chem. Phys* **1995**, *103*, 1702–1709. [CrossRef]
17. Jorgensen, W.L.; Tirado-Rives, J. The OPLS [optimized potentials for liquid simulations] potential functions for proteins, energy minimizations for crystals of cyclic peptides and crambin. *J. Am. Chem. Soc.* **1988**, *110*, 1657–1666. [CrossRef] [PubMed]
18. Jorgensen, W.L.; Madura, J.D.; Swenson, C.J. Optimized intermolecular potential functions for liquid hydrocarbons. *J. Am. Chem. Soc.* **1984**, *106*, 6638–6646. [CrossRef]
19. Bourque, A.J.; Rutledge, G.C. Kinetic Model for Layer-by-Layer Crystal Growth in Chain Molecules. *Macromolecules* **2016**, *49*, 3956–3964. [CrossRef]
20. Bourque, A.; Locker, C.R.; Rutledge, G.C. Molecular Dynamics Simulation of Surface Nucleation during Growth of an Alkane Crystal. *Macromolecules* **2016**, *49*, 3619–3629. [CrossRef]
21. Anwar, M.; Turci, F.; Schilling, T. Crystallization mechanism in melts of short n-alkane chains. *J. Chem. Phys.* **2013**, *139*, 214904. [CrossRef] [PubMed]
22. Yi, P.; Rutledge, G.C. Molecular simulation of crystal nucleation in n-octane melts. *J. Chem. Phys.* **2009**, *131*, 134902. [PubMed]
23. Yi, P.; Rutledge, G.C. Molecular simulation of bundle-like crystal nucleation from n-eicosane melts. *J. Chem. Phys* **2011**, *135*, 024903. [PubMed]
24. Hrahsheh, F.; Wilemski, G. Fluctuating structure of aqueous organic nanodroplets. *AIP Conf. Proc.* **2013**, *1527*, 63–66.
25. Yang, H.; Zhao, X.J.; Sun, M. Induced crystallization of single-chain polyethylene on a graphite surface: Molecular dynamics simulation. *Phys. Rev. B* **2011**, *84*, 011803. [CrossRef] [PubMed]
26. Kaner, P.; Ruiz-Orta, C.; Boz, E.; Wagener, K.B.; Tasaki, M.; Tashiro, K.; Alamo, R.G. Kinetic control of chlorine packing in crystals of a precisely substituted polyethylene. Toward advanced polyolefin materials. *Macromolecules* **2013**, *47*, 236–245. [CrossRef]

27. Wang, J.; Zhu, X.; Lu, X.; Zhou, Z.; Wang, G. On structures and properties of polyethylene during heating and cooling processes based on molecular dynamics simulations. *Comp. Theor. Chem.* **2015**, *1052*, 26–34. [CrossRef]
28. Yamamoto, T. Molecular dynamics of crystallization in n-alkane mixtures; texture, compatibility, and diffusion in crystals. *Polymer* **2016**, *99*, 721–733. [CrossRef]
29. Yi, P.; Locker, C.R.; Rutledge, G.C. Molecular dynamics simulation of homogeneous crystal nucleation in polyethylene. *Macromolecules* **2013**, *46*, 4723–4733. [CrossRef]
30. Modak, V.P.; Wyslouzil, B.E.; Singer, S.J. On the determination of the crystal-vapor surface free energy, and why a Gaussian expression can be accurate for a system far from Gaussian. *J. Chem. Phys.* **2016**, *145*, 054710. [CrossRef] [PubMed]
31. Obeidat, A.; Hrahsheh, F.; Wilemski, G. Scattering Form Factors for Russian Doll Aerosol Droplet Models. *J. Phys. Chem. B* **2014**, *119*, 9304–9311. [CrossRef] [PubMed]
32. Anwar, M.; Schilling, T. Crystallization of polyethylene: A molecular dynamics simulation study of the nucleation and growth mechanisms. *Polymer* **2015**, *76*, 307–312. [CrossRef]
33. Wang, E.; Escobedo, F.A. Mechanical Properties of Tetrapolyethylene and Tetrapoly (Ethylene Oxide) Diamond Networks Via Molecular Dynamics Simulations. *Macromolecules* **2016**, *49*, 2375–2386. [CrossRef]
34. Romanos, N.A.; Theodorou, D.N. Crystallization and melting simulations of oligomeric α1 isotactic polypropylene. *Macromolecules* **2010**, *43*, 5455–5469. [CrossRef]
35. Lee, S.; Rutledge, G.C. Plastic deformation of semicrystalline polyethylene by molecular simulation. *Macromolecules* **2011**, *44*, 3096–3108. [CrossRef]
36. Yi, P.; Rutledge, G.C. Molecular origins of homogeneous crystal nucleation. *Annu. Rev. Chem. Biomol. Eng.* **2012**, *3*, 157–182. [CrossRef] [PubMed]
37. Qiu, Y.; Molinero, V. Morphology of Liquid–Liquid Phase Separated Aerosols. *J. Am. Chem. Soc.* **2015**, *137*, 10642–10651. [CrossRef] [PubMed]
38. Molinero, V.; Moore, E.B. Water modeled as an intermediate element between carbon and silicon. *J. Phys. Chem. B* **2009**, *113*, 4008–4016. [CrossRef] [PubMed]
39. Malkin, T.L.; Murray, B.J.; Salzmann, C.G.; Molinero, V.; Pickering, S.J.; Whale, T.F. Stacking disorder in ice I. *Phys. Chem. Chem. Phys.* **2015**, *17*, 60–76. [CrossRef] [PubMed]
40. Moore, E.B.; Molinero, V. Is it cubic? Ice crystallization from deeply supercooled water. *Phys. Chem. Chem. Phys.* **2011**, *13*, 20008–20016. [CrossRef] [PubMed]
41. Moore, E.B.; de la Llave, E.; Welke, K.; Scherlis, D.A.; Molinero, V. Freezing, melting and structure of ice in a hydrophilic nanopore. *Phys. Chem. Chem. Phys.* **2010**, *12*, 4124–4134. [CrossRef] [PubMed]
42. Solveyra, E.G.; Llave, E.D.L.; Molinero, V.; Soler-Illia, G.J. A.A.; Scherlis, D.A. Structure, Dynamics, and Phase Behavior of Water in TiO_2 Nanopores. *J. Phys. Chem. C* **2013**, *117*, 3330–3342. [CrossRef]
43. Hudait, A.; Molinero, V. Ice crystallization in ultrafine water-salt aerosols: Nucleation, ice-solution equilibrium, and internal structure. *J. Am. Chem. Soc.* **2014**, *136*, 8081–8093. [CrossRef] [PubMed]
44. Johnston, J.C.; Molinero, V. Crystallization, melting, and structure of water nanoparticles at atmospherically relevant temperatures. *J. Am. Chem. Soc.* **2012**, *134*, 6650–6659. [CrossRef] [PubMed]
45. Lu, J.; Qiu, Y.; Baron, R.; Molinero, V. Coarse-Graining of TIP4P/2005, TIP4P-Ew, SPC/E, and TIP3P to Monatomic Anisotropic Water Models Using Relative Entropy Minimization. *J. Chem. Theory Comput.* **2014**, *10*, 4104–4120. [CrossRef] [PubMed]
46. Lupi, L.; Hudait, A.; Molinero, V. Heterogeneous nucleation of ice on carbon surfaces. *J. Am. Chem. Soc.* **2014**, *136*, 3156–3164. [CrossRef] [PubMed]
47. Moore, E.B.; Molinero, V. Structural transformation in supercooled water controls the crystallization rate of ice. *Nature* **2011**, *479*, 506–508. [CrossRef] [PubMed]
48. Moore, E.B.; Allen, J.T.; Molinero, V. Liquid-ice coexistence below the melting temperature for water confined in hydrophilic and hydrophobic nanopores. *J. Phys. Chem. C* **2012**, *116*, 7507–7514. [CrossRef]
49. Moore, E.B.; Molinero, V. Ice crystallization in water's "no-man's land". *J. Chem. Phys.* **2010**, *132*, 244504. [CrossRef] [PubMed]
50. Moore, E.B.; Molinero, V. Growing correlation length in supercooled water. *J. Chem. Phys.* **2009**, *130*, 244505. [CrossRef] [PubMed]
51. Hujo, W.; Shadrack Jabes, B.; Rana, V.K.; Chakravarty, C.; Molinero, V. The Rise and Fall of Anomalies in Tetrahedral Liquids. *J. Stat. Phys.* **2011**, *145*, 293–312. [CrossRef]

52. Kastelowitz, N.; Johnston, J.C.; Molinero, V. The anomalously high melting temperature of bilayer ice. *J. Chem. Phys.* **2010**, *132*, 124511. [CrossRef] [PubMed]
53. Xu, L.; Molinero, V. Is There a Liquid–Liquid Transition in Confined Water? *J. Phys. Chem. B* **2011**, *115*, 14210–14216. [CrossRef] [PubMed]
54. Nguyen, A.H.; Molinero, V. Identification of Clathrate Hydrates, Hexagonal Ice, Cubic Ice, and Liquid Water in Simulations: The CHILL+ Algorithm. *J. Phys. Chem. B* **2015**, *119*, 9369–9376. [CrossRef] [PubMed]
55. Nguyen, A.H.; Koc, M.A.; Shepherd, T.D.; Molinero, V. Structure of the Ice–Clathrate Interface. *J. Phys. Chem. C* **2015**, *119*, 4104–4117. [CrossRef]
56. Holten, V.; Limmer, D.T.; Molinero, V.; Anisimov, M.A. Nature of the anomalies in the supercooled liquid state of the mW model of water. *J. Chem. Phys.* **2013**, *138*, 174501. [CrossRef] [PubMed]
57. Bullock, G.; Molinero, V. Low-density liquid water is the mother of ice: On the relation between mesostructure, thermodynamics and ice crystallization in solutions. *Faraday Discuss.* **2013**, *167*, 371–388. [CrossRef] [PubMed]
58. González Solveyra, E.A.; de la Llave, E.; Scherlis, D.A.; Molinero, V. Melting and crystallization of ice in partially filled nanopores. *J. Phys. Chem. B* **2011**, *115*, 14196–14204. [CrossRef] [PubMed]
59. Reinhardt, A.; Doye, J.P.K. Effects of surface interactions on heterogeneous ice nucleation for a monatomic water model. *J. Chem. Phys.* **2014**, *141*, 084501. [CrossRef] [PubMed]
60. Factorovich, M.H.; Molinero, V.; Scherlis, D.A. A simple grand canonical approach to compute the vapor pressure of bulk and finite size systems. *J. Chem. Phys.* **2014**, *140*, 064111. [CrossRef] [PubMed]
61. Factorovich, M.H.; Molinero, V.; Scherlis, D.A. Vapor pressure of water nanodroplets. *J. Am. Chem. Soc.* **2014**, *136*, 4508–4514. [CrossRef] [PubMed]
62. Limmer, D.T.; Chandler, D. The putative liquid-liquid transition is a liquid-solid transition in atomistic models of water. *J. Chem. Phys.* **2011**, *135*, 134503. [CrossRef] [PubMed]
63. Limmer, D.T.; Chandler, D. The putative liquid-liquid transition is a liquid-solid transition in atomistic models of water. II. *J. Chem. Phys.* **2013**, *138*, 214504. [CrossRef] [PubMed]
64. Espinosa, J.R.; Vega, C.; Valeriani, C.; Sanz, E. Seeding approach to crystal nucleation. *J. Chem. Phys.* **2016**, *144*, 034501. [CrossRef] [PubMed]
65. Zaragoza, A.; Conde, M.M.; Espinosa, J.R.; Valeriani, C.; Vega, C.; Sanz, E. Competition between ices Ih and Ic in homogeneous water freezing. *J. Chem. Phys.* **2015**, *143*, 134504. [CrossRef] [PubMed]
66. Espinosa, J.R.; Sanz, E.; Valeriani, C.; Vega, C. Homogeneous ice nucleation evaluated for several water models. *J. Chem. Phys.* **2014**, *141*, 18C529. [CrossRef] [PubMed]
67. Bi, Y.; Cabriolu, R.; Li, T. Heterogeneous Ice Nucleation Controlled by the Coupling of Surface Crystallinity and Surface Hydrophilicity. *J. Phys. Chem. B* **2016**, *120*, 1507–1514. [CrossRef]
68. Cabriolu, R.; Li, T. Ice nucleation on carbon surface supports the classical theory for heterogeneous nucleation. *Phys. Rev. E* **2015**, *91*, 052402. [CrossRef] [PubMed]
69. Li, T.; Donadio, D.; Russo, G.; Galli, G. Homogeneous ice nucleation from supercooled water. *Phys. Chem. Chem. Phys.* **2011**, *13*, 19807–19813. [CrossRef] [PubMed]
70. Jacobson, L.C.; Molinero, V. A Methane−Water Model for Coarse-Grained Simulations of Solutions and Clathrate Hydrates. *J. Phys. Chem. B* **2010**, *114*, 7302–7311. [CrossRef] [PubMed]
71. Dhabal, D.; Nguyen, A.H.; Singh, M.; Khatua, P.; Molinero, V.; Bandyopadhyay, S.; Chakravarty, C. Excess entropy and crystallization in Stillinger-Weber and Lennard-Jones fluids. *J. Chem. Phys.* **2015**, *143*, 164512. [CrossRef] [PubMed]
72. Singh, M.; Dhabal, D.; Nguyen, A.H.; Molinero, V.; Chakravarty, C. Triplet Correlations Dominate the Transition from Simple to Tetrahedral Liquids. *Phys. Rev. Lett.* **2014**, *112*, 147801. [CrossRef] [PubMed]
73. Hudait, A.; Qiu, S.; Lupi, L.; Molinero, V. Free energy contributions and structural characterization of stacking disordered ices. *Phys. Chem. Chem. Phys.* **2016**, *18*, 9544–9553. [CrossRef] [PubMed]
74. Cox, S.J.; Kathmann, S.M.; Slater, B.; Michaelides, A. Molecular simulations of heterogeneous ice nucleation. I. Controlling ice nucleation through surface hydrophilicity. *J. Chem. Phys.* **2015**, *142*, 184704. [CrossRef] [PubMed]
75. Cox, S.J.; Kathmann, S.M.; Slater, B.; Michaelides, A. Molecular simulations of heterogeneous ice nucleation. II. Peeling back the layers. *J. Chem. Phys.* **2015**, *142*, 184705. [CrossRef] [PubMed]
76. Lupi, L.; Kastelowitz, N.; Molinero, V. Vapor deposition of water on graphitic surfaces: Formation of amorphous ice, bilayer ice, ice I, and liquid water. *J. Chem. Phys.* **2014**, *141*, 18C508. [CrossRef] [PubMed]

77. Fitzner, M.; Sosso, G.C.; Cox, S.J.; Michaelides, A. The Many Faces of Heterogeneous Ice Nucleation: Interplay Between Surface Morphology and Hydrophobicity. *J. Am. Chem. Soc.* **2015**, *137*, 13658–13669. [CrossRef] [PubMed]
78. Li, T.; Donadio, D.; Galli, G. Ice nucleation at the nanoscale probes no man's land of water. *Nat. Commun.* **2013**, *4*, 1887. [CrossRef] [PubMed]
79. Lu, J.; Chakravarty, C.; Molinero, V. Relationship between the line of density anomaly and the lines of melting, crystallization, cavitation, and liquid spinodal in coarse-grained water models. *J. Chem. Phys.* **2016**, *144*, 234507. [CrossRef] [PubMed]
80. Jabes, B.S.; Nayar, D.; Dhabal, D.; Molinero, V.; Chakravarty, C. Water and other tetrahedral liquids: Order, anomalies and solvation. *J. Phys. Condens. Matter* **2012**, *24*, 284116. [CrossRef] [PubMed]
81. Factorovich, M.H.; Gonzalez Solveyra, E.; Molinero, V.; Scherlis, D.A. Sorption Isotherms of Water in Nanopores: Relationship Between Hydropohobicity, Adsorption Pressure, and Hysteresis. *J. Phys. Chem. C* **2014**, *118*, 16290–16300. [CrossRef]
82. Limmer, D.T.; Chandler, D. Phase diagram of supercooled water confined to hydrophilic nanopores. *J. Chem. Phys.* **2012**, *137*, 044509. [CrossRef] [PubMed]
83. Haji-Akbari, A.; de Fever, R.S.; Sarupria, S.; Debenedetti, P.G. Suppression of sub-surface freezing in free-standing thin films of a coarse-grained model of water. *Phys. Chem. Chem. Phys.* **2014**, *16*, 25916–25927. [CrossRef] [PubMed]
84. Sun, H. COMPASS: An ab initio force-field optimized for condensed-phase applications overview with details on alkane and benzene compounds. *J. Phys. Chem. B* **1998**, *102*, 7338–7364. [CrossRef]
85. Plimpton, S. Fast Parallel Algorithms for Short-Range Molecular Dynamics. *J. Comput. Phys.* **1995**, *117*, 1–19. [CrossRef]
86. Berendsen, H.J.C.; Grigera, J.R.; Straatsma, T.P. The missing term in effective pair potentials. *J. Phys. Chem.* **1987**, *91*, 6269–6271. [CrossRef]
87. Goebel, A.; Lunkenheimer, K. Interfacial tension of the water/n-alkane interface. *Langmuir* **1997**, *13*, 369–372. [CrossRef]
88. Zeppieri, S.; Rodríguez, J.; López de Ramos, A.L. Interfacial Tension of Alkane + Water Systems. *J. Chem. Eng. Data* **2001**, *46*, 1086–1088. [CrossRef]
89. Nosé, S. A unified formulation of the constant temperature molecular dynamics methods. *J. Chem. Phys.* **1984**, *81*, 511–519. [CrossRef]
90. Hoover, W.G. Canonical dynamics: Equilibrium phase-space distributions. *Phys. Rev. A* **1985**, *31*, 1695–1697. [CrossRef]
91. Groom, C.R.; Bruno, I.J.; Lightfoot, M.P.; Ward, S.C. The Cambridge Structural Database. *Acta Crystallogr. Sect. B* **2016**, *72*, 171–179. [CrossRef] [PubMed]
92. Schneider, T.; Stoll, E. Molecular-dynamics study of a three-dimensional one-component model for distortive phase transitions. *Phys. Rev. B* **1978**, *17*, 1302–1322. [CrossRef]
93. Gloor, G.J.; Jackson, G.; Blas, F.J.; de Miguel, E. Test-area simulation method for the direct determination of the interfacial tension of systems with continuous or discontinuous potentials. *J. Chem. Phys.* **2005**, *123*, 134703. [CrossRef] [PubMed]
94. Steinhardt, P.; Nelson, D.; Ronchetti, M. Bond-orientational order in liquids and glasses. *Phys. Rev. B* **1983**, *28*, 784–805. [CrossRef]
95. Rozmanov, D.; Kusalik, P.G. Anisotropy in the crystal growth of hexagonal ice, I(h). *J. Chem. Phys* **2012**, *137*, 094702. [CrossRef] [PubMed]
96. Acree, W.E.; Chickos, J.S. Phase Transition Enthalpy Measurements of Organic and Organometallic Compounds. In *NIST Chemistry WebBook, NIST Standard Reference Database Number 69*; Linstrom, P.J., Mallard, W.G., Eds.; National Institute of Standards and Technology: Gaithersburg MD, USA, 2016.
97. Rolo, L.I.; Caço, A.I.; Queimada, A.J.; Marrucho, I.M.; Coutinho, J.A.P. Surface tension of heptane, decane, hexadecane, eicosane, and some of their binary mixtures. *J. Chem. Eng. Data* **2002**, *47*, 1442–1445. [CrossRef]
98. Viton, C.; Chavret, M.; Jose, J. Enthalpies of Vaporization of Normal Alkanes from Nonane to Pentadecane at Temperatures from 298 to 359 K. *ELDATA Int. Electron. J. Phys. Chem. Data* **1996**, *2*, 103.
99. Mondieig, D.; Rajabalee, F.; Metivaud, V.; Oonk, H.; Cuevas-Diarte, M. n-Alkane binary molecular alloys. *Chem. Mater.* **2004**, *16*, 786–798. [CrossRef]

100. Benet, J.; MacDowell, L.G.; Menduiña, C. Liquid-vapor phase equilibria and surface tension of ethane as predicted by the TraPPE and OPLS models. *J. Chem. Eng. Data* **2010**, *55*, 5465–5470. [CrossRef]
101. Wick, C.D.; Siepmann, J.I.; Schure, M.R. Molecular Simulation of Concurrent Gas−Liquid Interfacial Adsorption and Partitioning in Gas−Liquid Chromatography. *Anal. Chem.* **2002**, *74*, 3518–3524. [CrossRef] [PubMed]
102. Haji-Akbari, A.; Debenedetti, P.G. Thermodynamic and kinetic anisotropies in octane thin films. *J. Chem. Phys.* **2015**, *143*, 214501. [CrossRef] [PubMed]
103. Harris, J.G. Liquid-vapor interfaces of alkane oligomers: Structure and thermodynamics from molecular dynamics simulations of chemically realistic models. *J. Phys. Chem.* **1992**, *96*, 5077–5086. [CrossRef]
104. Kawamata, M.; Yamamoto, T. Molecular dynamics simulation of surface ordering in liquid n-alkanes. *J. Phys. Soc. Jpn.* **1997**, *66*, 2350–2354. [CrossRef]
105. Baron, R.; Molinero, V. Water-driven cavity-ligand binding: Comparison of thermodynamic signatures from coarse-grained and atomic-level simulations. *J. Chem. Theory Comput.* **2012**, *8*, 3696–3704. [CrossRef] [PubMed]
106. Yamamoto, T.; Nozaki, K.; Yamaguchi, A.; Urakami, N. Molecular simulation of crystallization in n-alkane ultrathin films: Effects of film thickness and substrate attraction. *J. Chem. Phys.* **2007**, *127*, 154704. [CrossRef] [PubMed]
107. Turnbull, D.; Fisher, J.C. Rate of nucleation in condensed systems. *J. Chem. Phys.* **1949**, *17*, 71–73. [CrossRef]
108. Young, T. An essay on the cohesion of fluids. *Philos. Trans. R. Soc. Lond.* **1805**, *95*, 65–87. [CrossRef]
109. Iwamatsu, M. Heterogeneous Nucleation on a Completely Wettable Substrate. In *Advances in Contact Angle, Wettability and Adhesion*; John Wiley & Sons, Inc.: Salem, MA, USA, 2013; pp. 49–72.
110. Auer, S.; Frenkel, D. Line tension controls wall-induced crystal nucleation in hard-sphere colloids. *Phys. Rev. Lett.* **2003**, *91*, 015703. [CrossRef] [PubMed]
111. Sirota, E.; Wu, X.; Ocko, B.; Deutsch, M. What Drives the Surface Freezing in Alkanes? *Phys. Rev. Lett.* **1997**, *79*, 531. [CrossRef]
112. Merkl, C.; Pfohl, T.; Riegler, H. Influence of the molecular ordering on the wetting of SiO_2/air interfaces by alkanes. *Phys. Rev. Lett.* **1997**, *79*, 4625. [CrossRef]
113. Volkmann, U.G.; Pino, M.; Altamirano, L.; Taub, H.; Hansen, F.Y. High-resolution ellipsometric study of an n-alkane film, dotriacontane, adsorbed on a SiO_2 surface. *J. Chem. Phys.* **2002**, *116*, 2107–2115. [CrossRef]